Mechanism and Kinetics of Ni-Y_2O_3-ZrO_2 Hydrogen Electrode for Water Electrolysis Reactions in Solid Oxide Electrolysis Cells

Weiping Pan,[a,b] Kongfa Chen,[b] Na Ai,[b] Zhe Lü,[c] and San Ping Jiang[b,z]

[a]*Institute of Optoelectronic Technology, Heilongjiang Institute of Technology, Harbin 15005, People's Republic of China*
[b]*Fuels and Energy Technology Institute & Department of Chemical Engineering, Curtin University, Perth, WA 6102, Australia*
[c]*Department of Physics, Harbin Institute of Technology, Harbin 150080, People's Republic of China*

Ni-Y_2O_3 stabilized ZrO_2 (Ni-YSZ) cermet is the most commonly used hydrogen electrode for hydrogen oxidation reaction (HOR) under solid oxide fuel cell (SOFC) mode and water reduction reaction (WRR) under solid oxide electrolysis cell (SOEC) mode. Here we studied the electrocatalytic activity of Ni-YSZ electrodes as a function of Ni content, water concentration and dc bias for WRR and HOR under SOEC and SOFC modes, respectively. The activity of Ni-YSZ cermet increases significantly with the increase of YSZ content due to the enhanced three phase boundaries (TPB). The electrode activity for the WRR and in less degree for the HOR increases with the increase of steam concentration. The electrode polarization resistance, R_E, for the WRR increases with the dc bias, while in the case of HOR, R_E decreases with the dc bias, demonstrating that kinetically the WRR and HOR is not reversible on the Ni-YSZ cermet electrodes under SOFC and SOEC operation modes. The WRR can be described by two electrode processes associated with the H_2O adsorption and diffusion on the oxygen-covered Ni or YSZ surface in the vicinities of TPB, followed by the charge transfer. The significant increase of high frequency electrode polarization resistance, R_H and in much less extent low frequency electrode polarization resistance, R_L with the dc bias indicates that the water electrolysis reaction is kinetically controlled by the reactant supply (e.g., the adsorbed H_2O species) limited charge transfer process.
 [DOI: 10.1149/2.0801602jes]

Manuscript submitted September 17, 2015; revised manuscript received November 13, 2015. Published November 25, 2015.

Solid oxide electrolysis cell (SOEC) as an electrochemical device to convert electricity of renewable energy sources such as solar energy, wind power, hydropower and geothermal power into chemical energy of fuels such as hydrogen and syngas has attracted increasing interests due to the depleting fossil fuel sources, high oil prices and environmental considerations.[1–7] In the case of water electrolysis to produce hydrogen, steam is introduced to the hydrogen electrode side where it is reduced to hydrogen, while the oxygen ions are migrated through the electrolyte to the air electrode side where they combine to form pure oxygen. Co-electrolysis of steam and CO_2 in an SOEC yields synthesis gas ($CO+H_2$) which in turn can be catalysed to various types of synthetic fuels (such as methane and methanol).[8–11] SOECs are reversible operation of solid oxide fuel cells (SOFCs), and therefore in principle the electrode and electrolyte materials developed for SOFCs can be utilized for SOECs.

Similar to SOFCs, Ni-yttria-stabilized zirconia (Ni-YSZ) cermets are the most common hydrogen electrodes for SOECs, due to its high electrical conductivity, high electrocatalytic activity, high thermal and structural stability and low price.[1,12–14] The incorporation of electrocatalytically active nanoparticles such as doped ceria oxides and Rh metal in the Ni-YSZ hydrogen electrodes enhances the ionic conductivity and three phase boundaries (TPBs), and thus substantially enhances the electrocatalytic activity and/or stability for the water electrolysis or water reduction reaction (WRR).[15–17] Nanostructured Ni infiltrated samaria doped ceria (SDC) can also increase the electrocatalytic activity by increasing the reaction area.[18,19]

The mechanism and kinetics of the hydrogen oxidation reaction (HOR) on Ni and Ni-YSZ cermet electrodes have been extensively studied.[20–27] Mizusaki et al. studied HOR on nickel patterned electrode on YSZ electrolyte and found that the rate of anodic reaction was essentially determined by the reaction of hydrogen and the adsorbed oxygen on the nickel surface.[26,28] Primdahl and Mogensen[29,30] studied the HOR on Ni-YSZ cermet anodes by impedance spectroscopy and the results indicate that the performance of the anodes critically depended on the cermet structure. The three phase boundary between YSZ, Ni and hydrogen reactant plays an important role for the HOR in SOFC. We also investigated in details the kinetics of HOR on the Ni-YSZ cermet electrodes of SOFC in moist H_2 environments.[22,27] The results revealed that the electrode reaction is controlled by at least two rate limiting processes, the electrode process associated with the hydrogen dissociative adsorption/diffusion on the surface of Ni particles and the one related to the hydrogen transfer from the Ni surface to the YSZ electrolyte surface, followed by a charge transfer process at the electrode and electrolyte interface.

There has been less study of mechanism and kinetics on Ni and Ni-YSZ cermet electrodes of WRR in SOEC.[2,20,31,32] Based on the symmetrical Ni-YSZ cermet electrodes, Dasari et al.[31] identified two frequency arcs for the water reduction reaction with the dominant middle or low frequency electrode process of possible gas-solid interaction. The electrochemical performance of Ni-YSZ cermet for the water electrolysis depends strongly on the steam concentration and 50% steam has been shown to have the minimum electrode impedance for the reaction on the cermet electrodes. On the other hand, on Ni-YSZ/YSZ/(La,Sr)MnO_3 solid oxide cells, deconvolution analysis of the impedance responses showed the water electrolysis could be limited by the charge transfer and surface diffusion on Ni-YSZ fuel electrodes.[33] Liang et al.[32] studied the electrochemical activity of Ni-YSZ cermet electrodes prepared by a new combustion method at 900 °C in 80% H_2O/20% H_2 and EIS results indicated that water adsorption and diffusion on the Ni-YSZ electrode are the limited step for the water electrolysis reaction. However, the reaction mechanism and kinetics of the WRR on Ni-YSZ cermet electrodes under SOEC mode is far from clear. In this paper, we report the results on the dependence of electrocatalytic activity of Ni-YSZ hydrogen electrodes as a function of operating temperature, water concentration and dc bias, and new reaction mechanism of water electrolysis reaction on Ni-YSZ cermet electrodes has been proposed.

Experimental

Electrolyte pellets were prepared by die pressing of 8 mol% Y_2O_3-stabilized ZrO_2 (YSZ, Tosoh) powder, followed by sintering at 1450°C for 5 h. The pellets were 1 mm in thickness and ~18 mm in diameter. NiO (J. T. Baker) and YSZ powders were ball-milled to form the NiO and NiO-YSZ composite electrode inks. The electrode compositions studied were 100% NiO, 80%NiO-20%YSZ and 50%NiO-50%YSZ in weight percentage, which gave the cermet composition of 100%Ni, 76%Ni-24%YSZ and 44%Ni-56%YSZ after the reduction of NiO to

[z]E-mail: s.jiang@curtin.edu.au

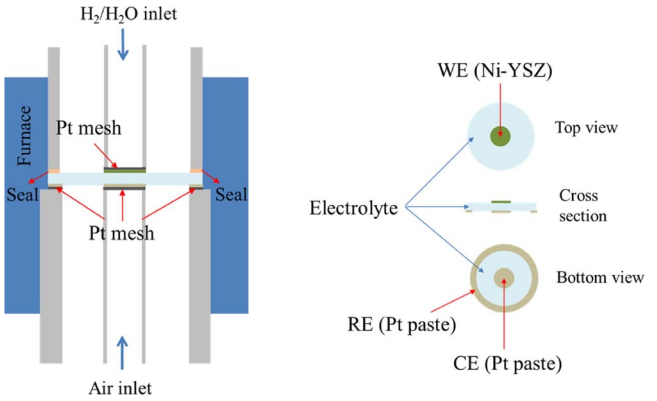

Figure 1. The schematic diagrams of cell configuration and setup.

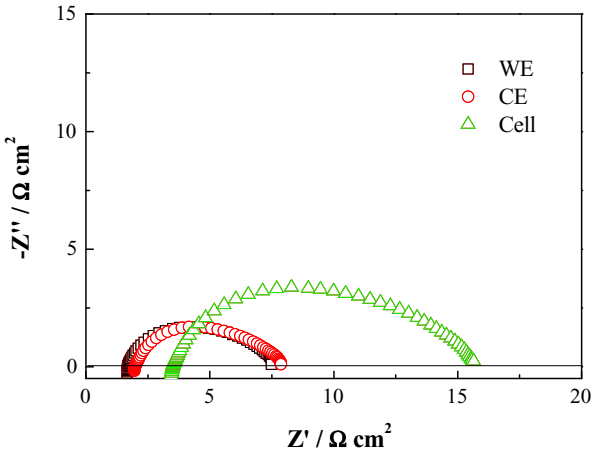

Figure 2. Impedance spectra of a LSM symmetric cell with three-electrode arrangement, measured under open circuit potential condition at 800°C.

Ni in the reducing environment. The reason of varying Ni content of Ni-YSZ cermet anodes was based on our early study of HOR on the Ni-YSZ cermet anodes.[22,27] In these studies, we have found that the Ni content plays an important role in the reaction kinetics but does not alter the reaction mechanism. With the increase of the Ni content in the Ni-YSZ cermet anodes, kinetically the reaction is increasingly limited to the three phase boundary at the electrode/electrolyte interface, and thus is beneficial for the fundamental study of the reaction mechanism. The origin of varying the Ni content in Ni-YSZ cermet anode is to magnify the electrode steps of the reaction under both SOFC and SOEC mode. The electrode ink was applied on the YSZ pellets by slurry coating and sintered at 1250°C for 2 h. The thickness of the electrode coating was 15∼30 μm and the electrode area was 0.5 cm^2 based on geometric surface area.

A three-electrode arrangement was used for the electrochemical measurement. Platinum paste (Pt ink 6082, Metalor) was applied as the counter and reference electrodes (RE). The counter electrode (CE) was painted symmetrically opposite to the working electrode (WE), and the reference electrode was painted as a ring around the counter electrode. The distance between the counter and reference electrodes was ∼4 mm. Figure 1 shows the cell configuration used in this study. The accurate separation of the electrode potential is critically related to the placement of reference electrode for the planar type cells.[34] Early studies show that cell configurations with symmetric electrode geometry and reference electrode positioned at the side of the working electrode and away from the exit of fuel and oxidant gases are suitable for the accurate performance evaluation of planar SOFCs and the cathodic and anodic polarization can be accurately separated if the thickness of the electrolytes is ≥ ∼250 μm).[35]

To verify the accuracy of the three-electrode configuration used in this study, we carried out the electrochemical impedance measurement on a $La_{0.8}Sr_{0.2}O_3$ (LSM, Fuel Cell Materials) symmetric cell with the same ring-shaped Pt reference electrode. The thickness of the YSZ electrolyte was ∼1 mm and LSM coating was 20–30 μm with an effective electrode area of 0.5 cm^2. Fig. 2 shows the impedance spectra of WE, CE and Cell of the LSM symmetric cell under open circuit potential condition at 800°C. The ohmic resistance between the reference electrode and LSM working electrode is the same as that between the reference electrode and LSM counter electrodes, ∼1.75 Ω cm^2, which equals to half of ∼3.50 Ω cm^2, measured between two LSM electrodes. This indicates that the equal potential line lies in the middle of the YSZ electrolyte. On the other hand, the electrode impedance measured between the Pt reference electrode and LSM working electrode overlaps with that measured between the reference and LSM counter electrode, again demonstrating reliability of the cell configuration used in this study in the measurement of the electrode impedance and polarization behavior.

Polarization curves in both SOFC and SOEC modes were conducted using a Gamry Reference 3000 Potentiostat. A current interruption technique was used to subtract the *iR* contribution during the polarization test. The electrochemical impedance responses under open circuit and different dc bias were measured in the frequency range from 0.1 Hz to 100 kHz with a signal amplitude of 5 mV. Electrode ohmic resistance R_Ω was obtained from the intercept of impedance spectra at high frequencies. The difference of the intercepts of impedance spectra with real axis at high frequency and low frequency ranges indicates the electrode polarization resistance, R_E. H_2 was selected as carrier gas to maintain the reducing environment in the hydrogen electrode. The steam concentration was 3 to 50% with the balanced H_2. The required amount of steam was generated by heating a saturator at a certain temperature. The microstructure of the electrodes was examined using Scanning electron microscopy (SEM Zeiss Neon 40EsB).

Results and Discussion

Effect of Ni content.— Figure 3 shows the SEM micrographs of surface and cross sections of the Ni and Ni-YSZ hydrogen electrodes with different Ni content. For pure Ni electrode, the Ni particles are seriously agglomerated into large particles in the size of 2 μm (Figs. 3a–3c). However, the gap between the Ni coating and YSZ electrolyte most likely occurred during the cooling process after the electrochemical test. In the case of Ni-YSZ composite electrode with 76 wt% Ni, the electrode structure is porous and consists of coarse and fine particles (Figs. 3d, 3e and 3f). The coarse particles in the size of 1 μm are Ni phase, while the fine particle in the size of 200 nm is YSZ phase. As the Ni content is reduced to 44 wt%, the electrode structure becomes finer with small Ni particles in the size of 0.5 μm (Figs. 3g, 3h and 3i). This indicates that the addition of YSZ particles reduces the Ni particle size and inhibits the growth and coarsening of Ni phase during the sintering at high temperatures. Qualitatively, the porosity of the cermet also decreased with the increase of Ni content in the cermet.

Figure 4 is the polarization and impedance curves of the Ni-YSZ hydrogen electrodes measured in SOFC and SOEC modes under 10% H_2O at 800°C. The polarization performance of Ni-YSZ cermet anodes depends strongly on the cermet composition. In the case of pure Ni electrode, the polarization performance is very poor. The current density at overpotential (η) of 0.2 V is about 0.01 mA cm^{-2} for both water reduction and hydrogen oxidation reactions (WRR and HOR). The electrochemical activity of the Ni based electrodes increases significantly with the addition of YSZ. The current density at $\eta = 0.2$ V is 0.04 and 0.23 mA cm^{-2} for the WRR and 0.09 and 0.31 mA cm^{-2} for the HOR on the 76%Ni-24%YSZ and 44%Ni-56%YSZ electrodes, respectively. This indicates that the presence of YSZ phase is critical to the electrode performance of the Ni electrodes most likely due to the substantially reduced Ni particles and enhanced TPBs.

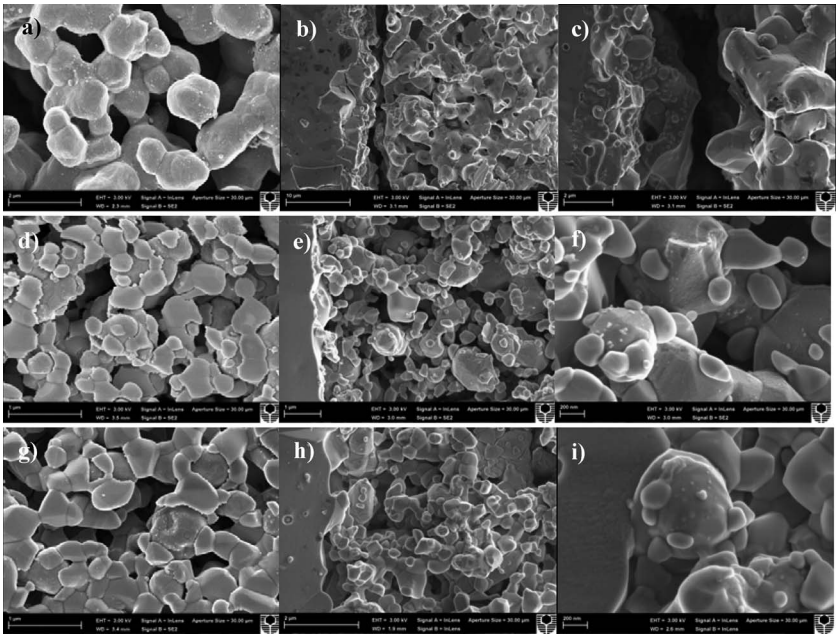

Figure 3. SEM micrographs of surface and cross section of Ni-YSZ hydrogen electrodes with (a, b, c) 100%, (d, e, f) 76% and (g, h, i) 44% Ni.

The electrochemical activity of the Ni-YSZ electrodes is supported by the impedance responses measured under open circuit conditions (Fig. 4b). For the reaction on Ni electrode, the impedance responses are characterized by a large and depressed arc, indicating the multi-steps limiting process.[22] The size of the impedance arcs decrease significantly for the reaction on Ni-YSZ cermet. R_E is 2.32 and 0.63 Ω cm^2 for the reaction on 76%Ni-24%YSZ and 44%Ni-56%YSZ electrodes, respectively, substantially smaller than 30.87 Ω cm^2 observed on Ni electrode. The very poor electrochemical performance of Ni is clearly due to the limited Ni electrode/YSZ electrolyte interface areas, as shown in Fig. 3. Addition of YSZ results in the reduction of the impedance in both the high and low frequency regions, and the effect is more dominant on the electrode impedance associated with low frequencies. The electrode ohmic resistance, R_Ω of 76%Ni-24%YSZ electrode is 1.0 Ωcm^2, lower than 1.65 Ωcm^2 measured on the 44%Ni-56%YSZ electrode. As the electrolyte thickness was kept constant at ∼1 mm, the decreased R_Ω of 76%Ni-24%YSZ electrode is likely due to the increased electrical conductivity of the electrode as the result of the increased Ni content in the cermet. In the case of pure Ni electrodes, R_Ω is 1.2 Ωcm^2, slightly higher than that of 76%Ni-24%YSZ electrode. This is most likely due to the significant agglomeration of the Ni electrode, leading to the poor microstructure and poor electrode and electrolyte interface contact (see Fig. 3).

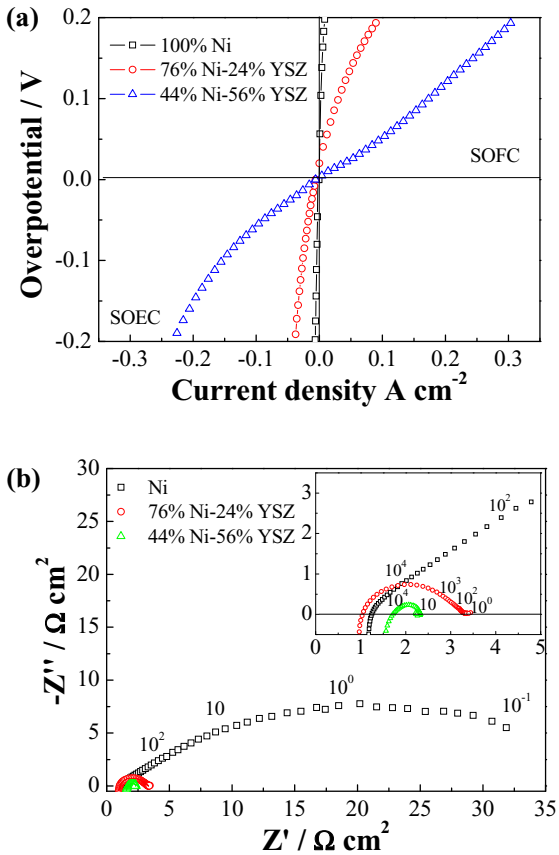

Figure 4. (a) *IR*-free current-overpotential curves and (b) impedance responses measured under open circuit of Ni and Ni-YSZ hydrogen electrodes under both SOFC and SOEC modes at 800°C in 10% H_2O/90%H_2.

Nickel provides the active surface for the HOR under the SOFC mode and WRR under the SOEC mode. As Ni is a predominantly electronic conductor, the electrochemical reaction is limited in a narrow region at the Ni/YSZ interface. On the other hand, in the case of cermet, the addition of YSZ phase not only increases the stability of the Ni electrodes but also significantly extends the TPB for the electrochemical reaction to the bulk of the electrode by forming a continuous and interconnected ionic pathway for oxide ions. In this study, the cermet with 44%Ni-56%YSZ shows good electrochemical activity, indicating the establishment of effective TPB and ionic/electronic pathways. This generally agrees well with the literature report of an optimum Ni concentration of 40–45 vol.%.[13,36,37]

Effect of steam concentration.— Cell potential values at zero current density correspond to the open circuit potential (OCP). The cell OCP is influenced by the steam/hydrogen ratio, according to the Nernst equation:

$$E = E^0 + \frac{RT}{2F} \ln\left(\frac{P_{H_2} P_{O_2}^{1/2}}{P_{H_2O}}\right) \quad [1]$$

where E^0 is the standard electrode potential, R is the universal gas constant, T is the absolute temperature (K), F is the Faraday constant, and P_{H_2}, P_{O_2} and P_{H_2O} denote the partial pressure of hydrogen, oxygen

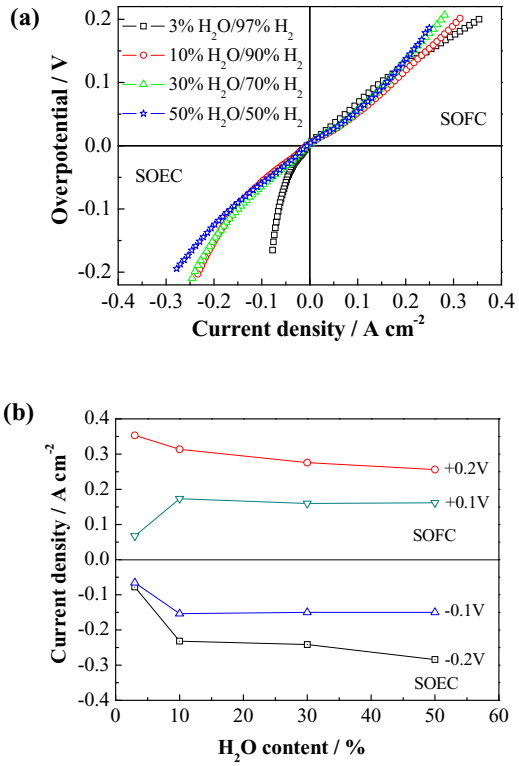

Figure 5. (a) *iR*-free current-overpotential curves of 44%Ni-56%YSZ hydrogen electrode and (b) corresponding plots of current densities measured at ±0.1 and ±0.2 V dc biases as a function of steam contents under SOFC and SOEC modes at 800°C.

and steam, respectively. The measured cell OCP was 1.04 V at 3% H_2O/97%H_2 and 0.90 V at 50% H_2O/50% H_2, which is close to the theoretical OCP of 1.10 V at 3% H_2O/97% H_2 and 0.94 V at 50% H_2O/50% H_2 calculated by Eq 1. This in turn indicates the good seal of the cells in this study.

Fig. 5a shows the *iR*-free polarization curves of 44%Ni-56%YSZ hydrogen electrode in both SOFC and SOEC operation modes under different steam contents at 800°C. In the SOEC mode, rapid increase of the η values is observed for the WRR at a low steam concentration of 3% H_2O, indicating the dominant concentration polarization. Increasing the steam content mitigates the rapid voltage loss and the η curves become more linear. With the steam concentration of 10 to 50%, the current densities are similar at low η and start to differentiate at η higher than 0.1 V. For the HOR under SOFC mode, the polarization losses are more or less similar at low current region. Different to that observed in the case of SOEC mode, the Ni-YSZ cermet electrode behaves better under low steam concentration fuels of 3% H_2O. This can also be seen more clearly from the plots of the current densities as a function of η values of 0.1 and 0.2 V for the reactions under SOFC and SOEC modes (Fig. 5b). In the SOEC mode, the current increases by increasing the steam content from 3% to 50%, while the current decreases with the increase of the steam content in the SOFC mode particularly at high η. This is understandable considering that steam is the reaction product of HOR under SOFC mode, but is the reactant of WRR under the SOEC mode. This clearly indicates that the polarization process for the high temperature solid oxide electrolysis is distinctively different from that of the fuel cell mode.

Effect of dc bias.— Figure 6 shows the impedance responses and plots of R_E as a function of dc bias under 50% H_2O at 800°C for the reaction on 76%Ni-24%YSZ and 44%Ni-56%YSZ electrodes. The impedance responses depend strongly on the dc bias and on the cermet composition. In the case of the 76%Ni-24%YSZ electrode, the size of the impedance arc decreases with the applied dc bias for the HOR under SOFC mode (Fig. 6b), consistent with the H_2 oxidation behavior on Ni-YSZ cermet anodes.[27] The significant effect of dc bias on the size of the impedance arc indicates the decrease of the reaction barrier for the charge transfer process of the HOR on Ni-YSZ cermet electrodes. In contrast to that under SOFC operation mode, the size of the impedance arc increases with the applied dc bias. For example, under open circuit, R_E is 2.36 Ω cm^2 and increases to 2.73 Ω cm^2 and 3.85 Ω cm^2 under dc bias of −30 and −150 mV, respectively (Fig. 6a). The increase in the R_E with dc bias under SOEC mode is almost linear in the dc bias range of 0 to 150 mV, similar to the linear decrease in the R_E with dc bias under SOFC mode (Fig. 6c). In the case of the 44%Ni-56%YSZ cermet electrode, the variation of impedance arcs as a function of applied dc bias becomes much smaller but the trend is similar to that observed for the reaction on the 76%Ni-44%YSZ cermet electrodes. The overall electrode polarization resistance is reduced with the applied dc bias under SOFC mode and increases under SOEC mode (Fig. 6f). The only difference is that the magnitude of the variation in R_E is much smaller, as compared to that measured on the 76%Ni-44%YSZ electrode (Fig. 6c). Under the SOEC operation mode, R_E is 0.85 Ω cm^2 at open circuit and increases to 0.92 Ω cm^2 under dc bias of −53 mV. Dasari et al. also observed the decrease of overall electrode polarization resistance in the SOFC mode and the increase in the electrolysis mode on symmetrical Ni-YSZ electrode cells in 3%H_2O/97%H_2.[31] The increase in the electrode polarization resistance was explained by the deficiency of H_2O due to low concentration of steam used. With the increase of water concentration to 50%, opposite trend of the overall electrode polarization resistance with dc bias was observed on the Ni-YSZ symmetrical cells.[31] Brisse et al. studied the impedance of commercial Ni-YSZ electrode supported solid oxide cells under dc bias and showed that the cell impedance change is very small under both SOFC and SOEC modes under low dc currents of 0.33 A cm^{-2}, but the overall cell impedance increases more rapidly under SOEC mode when large dc current was applied.[38] However, as pointed by the author, impedance alone cannot distinguish the limitations or the changes occur at the hydrogen or oxygen electrode side.

The equivalent circuit of two RQ units in series was used to analyze the impedance responses of the reaction on Ni-YSZ electrodes under SOFC and SOEC modes (Fig. 6g). In the circuit, L corresponds to an inductance, which is usually associated with the long Pt current/voltage probes and the heating elements of the furnace. R_Ω is the ohmic resistance between the working and reference electrodes. Q and R represent constant phase element and electrode polarization resistance, respectively and subscripts H and L correspond to the high and low frequency arcs. Such equivalent circuit has been used in the fitting of the impedance responses of the HOR[27] and WRR[31] on Ni and Ni-YSZ cermet electrodes.

Figures 7a and 7b show the examples of the fitting results for HOR under SOFC mode at dc bias of 37 mV and for WRR under SOEC mode at dc bias of −30 mV at 800°C, respectively, on a 76%Ni-24%YSZ cermet electrode. The solid lines are fitted results and symbols are experimental data. The fitting between the measured and calculated impedance data is quite reasonable, indicating the applicability of the equivalent circuit for the HOR under SOFC and WRR under SOEC modes on Ni-YSZ cermet electrodes. Table I lists impedance parameters of the 76%Ni-24%YSZ electrode as a function of dc bias for HOR and WRR measured at 800°C under 50%H_2O/50%H_2. For the HOR on the Ni-YSZ cermet electrode under SOFC mode, R_H decreases with the applied dc bias while the changes in the R_L are negligible (Fig. 7c). This is in good agreement with early study of the HOR on Ni and Ni-YSZ cermet anodes,[22,27] indicating that electrode process associated with high frequencies is controlled by the charge transfer step and the one associated with the low frequencies is most likely related to the hydrogen dissociation and diffusion process.

Ni-YSZ cermet electrode behaves differently for the WRR under the SOEC mode. In opposite to that observed under SOFC mode, R_H increases significantly with the applied dc bias with the slope of 7.24 Ωcm^2 V^{-1} (Fig. 7c). Also, very different to the negligible change of

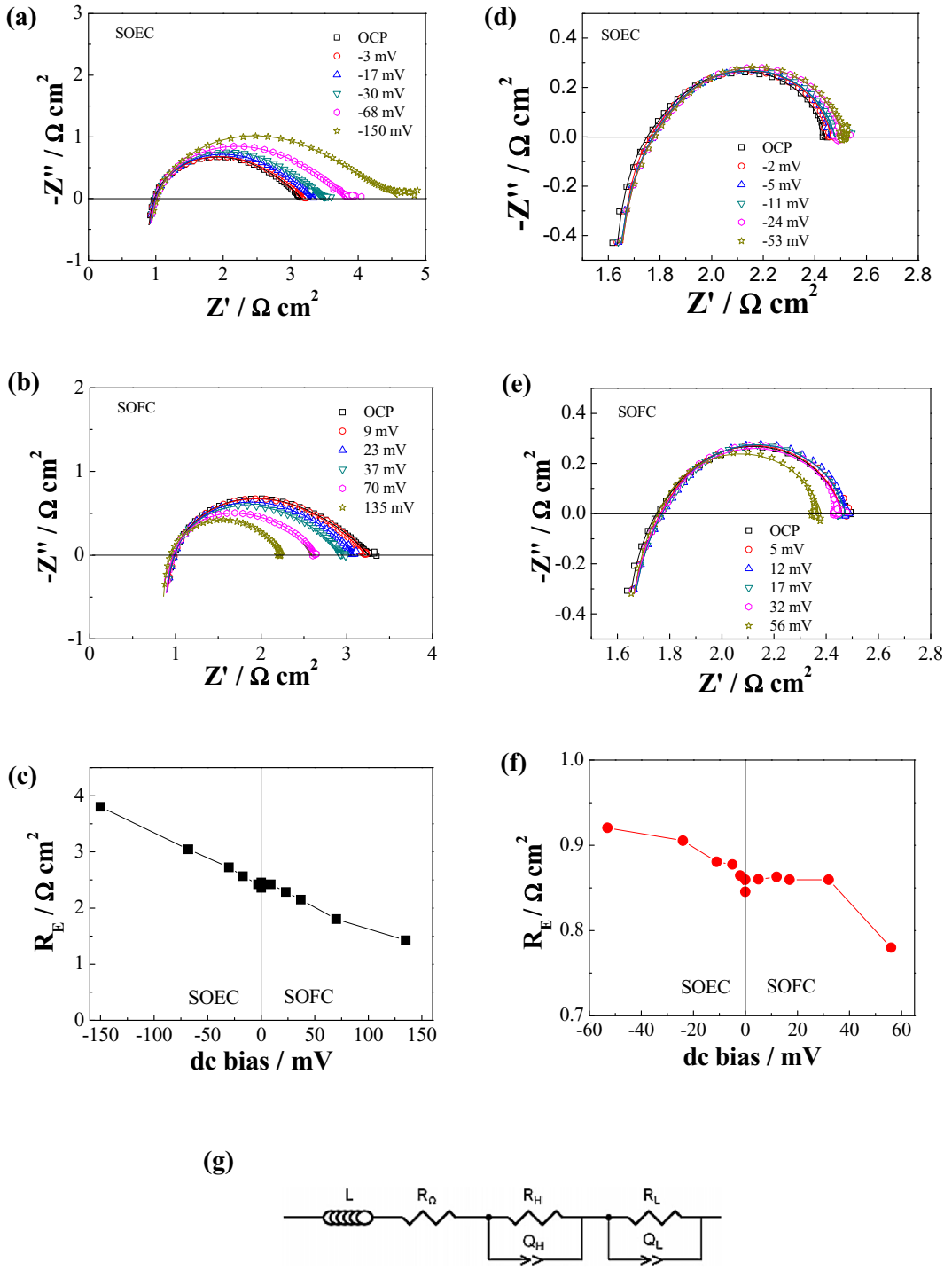

Figure 6. Impedance responses and plots of R_E as a function of dc bias on (a, b, c) 76%Ni-24%YSZ electrodes and on (d, e, f) 44% Ni-56%YSZ electrode, measured at 800°C in 50% H_2O/50% H_2 under SOFC and SOEC modes. Symbols are the experimental data and lines are the fitted results. Equivalent circuit employed to fit the impedance data is given in (g).

R_L for the HOR under SOFC mode, R_L also increases with the dc bias though the magnitude of the increase is relatively much smaller, 2.31 $\Omega cm^2\ V^{-1}$. This implies that the electrode processes associated with high and low frequencies are both charge transfer related. As shown previously, addition of YSZ phase to the Ni cermet will not change the reaction mechanism but will have significant effect on the kinetics of the individual reaction steps.[27] Thus, it would be expected that similar reaction steps also occur on 44%Ni-56%YSZ cermet electrodes for the reaction under both SOFC and SOEC modes. The increase rather than decrease of the electrode polarization resistance implies that both electrode steps associated with the high and low frequencies are not controlled by the charge transfer process. The very different dc bias dependence of the electrode polarization resistance clearly indicates that the reaction mechanism of WRR is very different from that of HOR.

Effect of temperature.— Figure 8a is the *iR*-free polarization curves of 44%Ni-56%YSZ cermet electrode measured under SOFC and

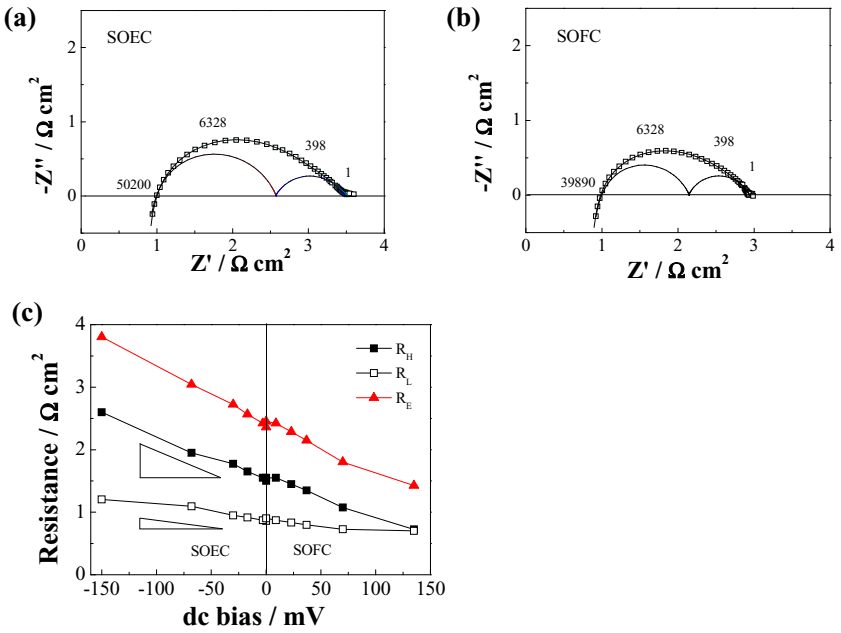

Figure 7. Impedance curves for the reaction on a 76%Ni-24%YSZ hydrogen electrode measured under (a) SOEC mode at dc bias of −30 mV and (b) SOFC mode at dc bias of 37 mV. Symbols are experimental data and lines are the fitted results. Plots of R_E, R_H and R_L as a function of dc bias measured at 800°C under 50%H_2O/50%H_2 are given in (c).

SOEC modes at different temperatures in 50%H_2O/50%H_2. The overpotential loss decreases with increasing of temperature for the reaction in both SOFC and SOEC modes, indicating that both HOR and WRR are thermally activated processes. Figure 8b shows the impedance spectra of 44%Ni-56%YSZ cermet electrode at open circuit conditions under different temperatures in 50%H_2O/50%H_2. R_E of 44%Ni-56%YSZ from 0.85 Ω cm² at 800°C increases to 3.40 Ω cm² at 650°C. Table II shows impedance parameters of 44%Ni-56%YSZ electrode under open circuit potential condition with 50%H_2O/50%H_2 at different temperatures. The size of high frequency arc increases significantly with the decrease in temperature, indicating that the charge transfer process strongly depends on temperature.[39] This also indicates that electrode process associated with the high frequencies is most likely related to the charge transfer process. At low temperature of 700 °C, the impedance responses are characterized by two clearly separated arcs at high and low frequencies. This further verifies the applicability of the equivalent circuit of Fig. 6g used in the present study.

Table I. Impedance parameters of 76%Ni/24%YSZ electrode as a function of dc bias at SOEC and SOFC modes measured at 800°C under 50%H_2O/50%H_2.

	High frequency arc		Low frequency arc	
dc bias/mV	R_H/Ω cm²	C_H/μF cm^{-2}	R_L/Ω cm²	C_L/μF cm^{-2}
	Solid oxide electrolysis cells			
0	1.50	20.32	0.86	181.14
−3	1.55	19.75	0.87	190.50
−17	1.65	19.12	0.92	205.91
−30	1.78	18.24	0.95	238.85
−68	1.95	17.18	1.10	197.23
−150	2.60	15.75	1.20	569.57
	Solid oxide fuel cells			
0	1.55	21.66	0.90	229.34
9	1.55	19.71	0.87	191.03
23	1.45	19.75	0.84	186.68
37	1.35	20.26	0.80	187.77
70	1.08	21.98	0.73	212.94
135	0.73	38.88	0.70	100.77

Figure 9 shows activation energy plots of the electrode polarization resistance associated with high and low frequency arcs at open circuit condition for the reaction on the 44%Ni-56%YSZ and 76%Ni-24%YSZ electrodes in 50% H_2O/50%H_2. The activation energy of the electrode process associated with high frequencies is 124 and 142 kJ mol^{-1} (1.29 and 1.47 eV) for 44%Ni-56%YSZ and 76%Ni-24%YSZ

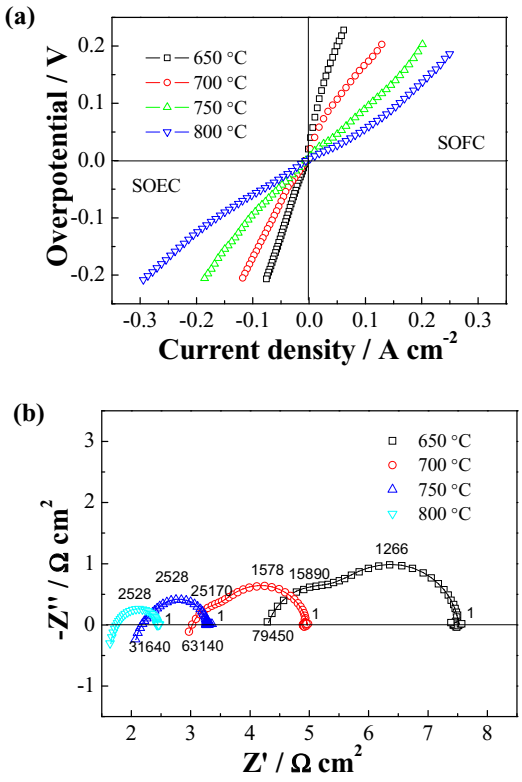

Figure 8. (a) *IR*-free current-overpotential curves and (b) impedance spectra measured at open circuit potential on a 44%Ni-56%YSZ hydrogen electrode at different temperatures under 50% H_2O/50%H_2.

Table II. Impedance parameters of 44%Ni-56%YSZ electrode under open circuit potential condition with 50%H_2O/50%H_2 at different temperatures.

	High frequency arc		Low frequency arc	
	$R_H/\Omega\ cm^2$	$C_H/\mu F\ cm^{-2}$	$R_L/\Omega\ cm^2$	$C_L/\mu F\ cm^{-2}$
800°C	0.18	20.25	0.67	85.78
750°C	0.30	15.45	0.99	52.85
700°C	0.83	5.45	1.35	75.01
650°C	1.55	4.83	1.85	81.88

electrodes, respectively. On the other hand, for the electrode process associated with low frequencies, R_L, it is 55 and 56 kJ mol^{-1} (0.57 and 0.58 eV) for the reaction of 44%Ni-56%YSZ and 76%Ni-24%YSZ electrodes, respectively, significantly smaller than 124 and 142 kJ mol^{-1} measured for the high frequency electrode steps. The electrode process associated with the adsorption and diffusion steps has a much lower activation energy than the charge-transfer process. The high activation energy value of R_H observed in this study again indicates that the electrode process associated with high frequencies is a charge transfer reaction at the TPB, close to that of the HOR at the Ni-YSZ cermet electrode.[27]

Reaction mechanism and kinetics.— There have been many studies on the mechanism and kinetics for the HOR of Ni and Ni-YSZ cermet electrodes.[20–24,28] In moist H_2, the impedance responses of the Ni-based electrodes show the existence of one or more (up to three) arcs,[20–22,28] indicating the contribution of several reaction steps to the overall hydrogen oxidation reaction. Our early studies show that the electrode process for the HOR can be described by two electrode steps associated with low and high frequency arcs; the electrode process associated with low frequency arc has been attributed to hydrogen dissociation adsorption/diffusion on the surface of Ni, and the one associated with high frequency arc is the process of hydrogen transfer from the Ni/YSZ surface to the TPB region, followed by the charge transfer process at TPB.[22,27] The reaction steps for the HOR can be written as follows:[27]

$$H_2\ (g) + 2S_m\ (+/\text{or}\ O\text{-}S_m) \rightarrow 2H_{ad}\text{-}S_m\ (+/\text{or}\ H_{ad}\text{-}O\text{-}S_m) \quad [2]$$

$$H_{ad}\ \text{-}\ S_m\ (+/\text{or}\ H_{ad}\ \text{-}O\text{-}\ S_m) \rightarrow H_{ad,YSZ}\ (TPB) + S_m\ (+/\text{or}\ O\text{-}S_m) \quad [3]$$

$$O^{2-}_{YSZ} + 2H_{ad,YSZ} \xrightarrow{TPB} H_2O + 2e_{Ni} + V_{\ddot{O}} \quad [4]$$

The overall HOR is thus:

$$H_2 + O^{2-}_{YSZ} \rightarrow H_2O + 2e_{Ni} + V_{\ddot{O}} \quad [5]$$

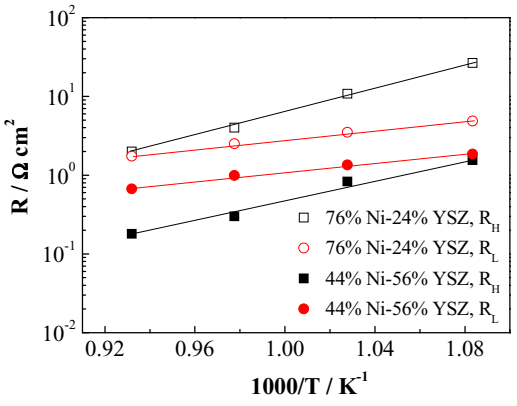

Figure 9. Activation energy plots of the electrode polarization resistance of R_H and R_L on 44%Ni-56%YSZ and 76%Ni-24%YSZ cermet electrodes at open circuit condition under 50% H_2O/50%H_2.

where O^{2-}_{YSZ} is an oxygen ion on YSZ lattice, $V_{\ddot{O}}$ is an oxygen vacancy on the YSZ surface, S_m is an active Ni metal surface site and O-S_m is an active metal surface site adjacent to an adsorbed oxygen, O_{ad}, for the dissociation of H_2O or H_2 and e_{Ni} is an electron on the electrical conducting Ni surface near TPB. The presence of water can greatly increase the O-S_m sites by the direct H_2O-Ni interaction at high temperatures. This is supported by the report that the electrode impedance for HOR is substantially reduced in the presence of water as compared to that in dry H_2.[22] Steps 2 and 3 are associated with the process of hydrogen dissociation and diffusion, facilitated by the hydrogen spillover mechanism.[22,27,40] Step 4 is the charge transfer process. The high frequency electrode process of the charge transfer steps is supported by the observations that the R_H shows significant decrease with the applied dc bias and strong dependence on the temperature with activation energy of 124 and 142 kJ mol^{-1} (Figs. 7 and 9). The strong dependence of the R_H on temperature is typically associated with charge transfer process.[30] R_L for HOR is essentially independent of applied dc bias and shows much less dependence on temperature (Figs. 7 and 9). The results of the present study are consistent with that reported earlier.[22]

In principle, the WRR is the reverse process of Reaction 5 for HOR. Similar to HOR, the reaction of Ni-YSZ cermet electrodes for WRR under SOEC mode can also be described by two electrode processes associated with high and low frequencies, R_H and R_L. However, very different to that under fuel cell mode, the electrode polarization resistance of low and high frequency arcs behaves very differently in respect to the steam concentration and dc bias. R_E for the WRR decreases with the increase of water concentration above 3% while R_E for HOR is more or less independent of water concentration from 3 to 50%. This is understandable as the H_2 concentration is sufficiently high, 97 to 50%, to sustain the hydrogen oxidation reaction. The significant increase in the R_H with the applied dc bias implies that the electrode process associated with the high impedances is also affected with the charge transfer process, however very different from that in the case of HOR,[22,27] the significant increase in R_H with the dc bias implies the increased reaction barrier of the electrode process under the polarization, an indication of the deficient or insufficient reactant supply proceeding to the charge transfer steps. The much slow increase of the R_L with the dc bias indicates that electrode process associated with the low frequency arc is also related to the charge transfer but in a much less extent. The capacitive components of the electrode processes associated with the low and high frequencies are in the double layer capacitance range of 10^{-4} to 10^{-5} F cm^{-2} (see Table I), which could be related to the ionic transfer and/or charge transfer processes.[41]

The first step for the WRR must be the adsorption and dissociation of the water molecules on the surface of Ni-YSZ cermet electrodes. Ge et al.[42] proposed the H_2O adsorption at TPB, followed by the dissociation of H_2O into adsorbed hydrogen and hydroxide species (H_{ad} and OH^-) and H_2 is produce by the combination of two H_{ad}. On the other hand, Dasari et al.[31] considered that direct interaction between H_2O gas molecules and Ni-YSZ electrodes leads to the dissociation into atomic O and H_2, and the atomic oxygen is reduced by accepting two electrons from Ni electrodes and incorporated into YSZ electrolyte at the electrode/electrolyte interface. This is largely based on the report that interaction between H_2O and Ni(110) leads to the complete dissociation of H_2O with no detection of adsorbed water molecules, hydroxide or hydroxyl species.[43] However, H_2O adsorption could occur on oxygen covered Ni surface at elevated temperatures.[44] Gorski et al. studied the mechanism of H_2O dissociation on YSZ surface using temperature-programmed desorption (TPD) spectroscopy and density functional theory (DFT) and showed that interaction of H_2O with YSZ results in dissociative adsorption, forming OH surface species.[45] This indicates that adsorption of gaseous H_2O could occur on oxygen-covered Ni or YSZ surface close to the TPB as the first step of WRR, but the residence time of the adsorbed H_2O molecules, H_2O_{ad} could be very short. This is due to the fact that thermodynamically gaseous H_2O molecules are much more stable than the adsorbed one. The adsorption and desorption processes of H_2O molecules can be represented

as follows:

$$H_2O\ (gas) + O - S_m \overset{slow}{\rightarrow} H_2O_{ad} - O - S_m \overset{fast}{\rightarrow} H_2O\ (gas) + O - S_m \quad [6]$$

$$H_2O_{ad}\text{-}O\text{-}S_m \rightarrow H_2O_{ad,TPB} \quad [7]$$

Here O-S_m represents oxygen-covered Ni or YSZ surface site or active metal surface site adjacent to an adsorbed oxygen, O_{ad}, for the dissociation of H_2O or H_2. The H_2O_{ad} at TPB (reaction 7) would be directly dissociated into H_2 and O (i.e., the reverse reaction 5) or OH species by accepting two electrons:

$$H_2O_{ad,TPB} + 2e_{Ni} + V_{\ddot{O}} \rightarrow H_2 + O^{2-}_{YSZ} \quad [8]$$

Or

$$H_2O_{ad,TPB} \rightarrow OH_{YSZ} + H_{Ni} \quad [9]$$

$$2OH_{YSZ} + 2e_{Ni} + V_{\ddot{O}} \rightarrow O^{2-}_{YSZ} + 2H_{Ni} \quad [10]$$

$$H_{Ni} + H_{Ni} \rightarrow H_2 \quad [11]$$

The electrode process associated with low frequency arc could be the water adsorption and diffusion on oxygen-covered Ni or YSZ surface, i.e., reactions 6 and 7, while the one at high frequency arc corresponds to the charge transfer steps of reactions 8 or 10. As shown in Fig. 7, R_H and in less extent R_L for WRR under the SOEC mode increases with the dc bias. The increased reaction barrier under the influence of the polarization implies that the charge transfer reactions 8 or 10 for WRR would be limited by the supply of reactant, either $H_2O_{ad,TPB}$ or OH_{YSZ} species. This can be understood from the thermodynamic point of view that in reaction 6, the adsorption of gaseous H_2O could be a slow and weak process while the desorption of the adsorbed species, H_2O_{ad}, would be a fast process under the SOEC operation conditions, resulting in an extremely short residential time of the adsorbed H_2O_{ad}-O-S_m species and thus an insufficient reactant supply to the TPB region for the reaction. The reactant supply-limited charge transfer process for WRR is also supported by the observed decrease of the cell resistance with the increase in electrolysis current density on $La_{0.75}Sr_{0.25}Cr_{0.5}Mn_{0.5}O_3$ (LSCM) hydrogen electrode, measured at 800–850°C.[46] In the case of LSCM hydrogen electrode, the residence time of H_2O_{ad} could be sufficiently high due to the faster adsorption rate of H_2O on the oxide surface, as compared to the oxygen-covered Ni, resulting in the increased dominance of the charge transfer process for the WRR on the oxide-based electrodes like LSCM. The strong dependence of the R_E on the dc bias under high steam concentration of 50% (Fig. 6) also indicates that gas diffusion does not contribute significantly to the kinetics of the water electrolysis on Ni-YSZ hydrogen electrodes, except in the case where the steam concentration is very low, e.g., 3%H_2O.

Conclusions

Electrocatalytic activity of Ni-YSZ hydrogen electrodes is dependent on Ni content, operating temperature, water concentration and dc bias for the water reduction reaction (WRR) under SOEC mode and hydrogen oxidation reaction (HOR) under SOFC mode. The impedance behavior for HOR and WRR on Ni-YSZ electrodes is characterized by two separable impedance arcs at high and low frequencies, indicating HOR and WRR on Ni-YSZ electrode are controlled by two rate limiting processes. For HOR at SOFC mode, R_H shows significant decrease with the applied dc bias and strong dependence on temperature. The strong dependence of the R_H on temperature is typically associated with charge transfer process. R_L is essentially independent of applied dc bias and shows much less dependence on temperature, characteristics of chemical process associated with hydrogen dissociation adsorption/diffusion. For WRR at SOEC mode, the first step of the reaction is the adsorption of gaseous H_2O on oxygen-covered Ni at the TPB, followed by the dissociation, surface diffusion and charge transfer steps at the electrode/electrolyte interface. The electrode polarization resistance associated with high and low frequencies, R_H and R_L for WRR increases with the dc bias, indicating the increased reaction barrier for the WRR under polarization. The significant increase of R_H and in much less extent R_L with the dc bias indicates that charge transfer reaction for WRR is limited by the supply of reactant due to the very short residence time of the adsorbed H_2O_{ad} species in the vicinities of the TPB region.

Acknowledgments

The project is supported by Doctoral Research Fund Program of Heilongjiang Institute of Technology (2012BJ22), Curtin University Research Fellow Program and the Australian Research Council (DP150102025). The authors acknowledge the facilities, scientific and technical assistance of the Curtin University Microscopy & Microanalysis Facility, which is partially funded by the University, State and Commonwealth Governments.

References

1. M. A. Laguna-Bercero, *J. Power Sources*, **203**, 4 (2012).
2. A. Hauch, S. D. Ebbesen, S. H. Jensen, and M. Mogensen, *J. Electrochem. Soc.*, **155**, B1184 (2008).
3. C. Graves, S. D. Ebbesen, and M. Mogensen, *Solid State Ionics*, **192**, 398 (2011).
4. T. Ishihara and T. Kanno, *ISIJ International*, **50**, 1291 (2010).
5. C. M. Stoots, J. E. O'Brien, K. G. Condie, and J. J. Hartvigsen, *Int. J. Hydrog. Energy*, **35**, 4861 (2010).
6. A. Hauch, S. D. Ebbesen, S. H. Jensen, and M. Mogensen, *Journal of Materials Chemistry*, **18**, 2331 (2008).
7. A. Hauch, S. H. Jensen, S. Ramousse, and M. Mogensen, *J. Electrochem. Soc.*, **153**, A1741 (2006).
8. S. D. Ebbesen and M. Mogensen, *Journal of Power Sources*, **193**, 349 (2009).
9. S. D. Ebbesen, R. Knibbe, and M. Mogensen, *Journal of The Electrochemical Society*, **159**, F482 (2012).
10. C. M. Stoots, J. E. O'Brien, J. S. Herring, and J. J. Hartvigsen, *Journal of Fuel Cell Science and Technology*, **6**, 011014 (2009).
11. W. Li, H. Wang, Y. Shi, and N. Cai, *International Journal of Hydrogen Energy*, **38**, 11104 (2013).
12. M. Ni, M. K. H. Leung, and D. Y. C. Leung, *Int. J. Hydrog. Energy*, **33**, 2337 (2008).
13. S. P. Jiang and S. H. Chan, *J. Mater. Sci.*, **39**, 4405 (2004).
14. W. Z. Zhu and S. C. Deevi, *Mater. Sci. Eng. A-Struct. Mater. Prop. Microstruct. Process.*, **362**, 228 (2003).
15. P. Kim-Lohsoontorn, Y.-M. Kim, N. Laosiripojana, and J. Bae, *Int. J. Hydrog. Energy*, **36**, 9420 (2011).
16. Y. Chen, J. Bunch, C. Jin, C. H. Yang, and F. L. Chen, *Journal of Power Sources*, **204**, 40 (2012).
17. A. R. Hanifi, M. A. Laguna-Bercero, T. H. Etsell, and P. Sarkar, *Int. J. Hydrog. Energy*, **39**, 8002 (2014).
18. N. Osada, H. Uchida, and M. Watanabe, *J. Electrochem. Soc.*, **153**, A816 (2006).
19. H. Uchida, N. Osada, and M. Watanabe, *Electrochem. Solid State Lett.*, **7**, A500 (2004).
20. A. M. Sukeshini, B. Habibzadeh, B. P. Becker, C. A. Stoltz, B. W. Eichhorn, and G. S. Jackson, *J. Electrochem. Soc.*, **153**, A705 (2006).
21. A. Bieberle and L. J. Gauckler, *Solid State Ionics*, **135**, 337 (2000).
22. S. P. Jiang and S. P. S. Badwal, *J. Electrochem. Soc.*, **144**, 3777 (1997).
23. W. G. Bessler, M. Vogler, H. Stormer, D. Gerthsen, A. Utz, A. Weber, and E. Ivers-Tiffee, *Phys. Chem. Chem. Phys.*, **12**, 13888 (2010).
24. C. W. Sun and U. Stimming, *J. Power Sources*, **171**, 247 (2007).
25. A. Ehn, J. Ho/gh, M. Graczyk, K. Norrman, L. Montelius, M. Linne, and M. Mogensen, *Journal of The Electrochemical Society*, **157**, B1588 (2010).
26. J. Mizusaki, H. Tagawa, T. Saito, K. Kamitani, T. Yamamura, K. Hirano, S. Ehara, T. Takagi, T. Hikita, M. Ippommatsu, S. Nakagawa, and K. Hashimoto, *J. Electrochem. Soc.*, **141**, 2129 (1994).
27. S. P. Jiang and S. P. S. Badwal, *Solid State Ionics*, **123**, 209 (1999).
28. J. Mizusaki, H. Tagawa, T. Saito, T. Yamamura, K. Kamitani, K. Hirano, S. Ehara, T. Takagi, T. Hikita, M. Ippommatsu, S. Nakagawa, and K. Hashimoto, *Solid State Ionics*, **70**, 52 (1994).
29. S. Primdahl, B. F. Sorensen, and M. Mogensen, *J. Am. Ceram. Soc.*, **83**, 489 (2000).
30. S. Primdahl and M. Mogensen, *J. Electrochem. Soc.*, **144**, 3409 (1997).
31. H. P. Dasari, S. Y. Park, J. Kim, J. H. Lee, B. K. Kim, H. J. Je, H. W. Lee, and K. J. Yoon, *J. Power Sources*, **240**, 721 (2013).
32. M. D. Liang, B. Yu, M. F. Wen, J. Chen, J. M. Xu, and Y. C. Zhai, *Int. J. Hydrog. Energy*, **35**, 2852 (2010).
33. E. C. Shin, P. A. Ahn, H. H. Seo, J. M. Jo, S. D. Kim, S. K. Woo, J. H. Yu, J. Mizusaki, and J. S. Lee, *Solid State Ionics*, **232**, 80 (2013).

34. S. B. Adler, *J. Electrochem. Soc.*, **149**, E166 (2002).
35. S. P. Jiang, *J. Appl. Electrochem.*, **34**, 1045 (2004).
36. J. H. Lee, J. W. Heo, D. S. Lee, J. Kim, G. H. Kim, H. W. Lee, H. S. Song, and J. H. Moon, *Solid State Ionics*, **158**, 225 (2003).
37. J. H. Lee, H. Moon, H. W. Lee, J. Kim, J. D. Kim, and K. H. Yoon, *Solid State Ionics*, **148**, 15 (2002).
38. A. Brisse, J. Schefold, and M. Zahid, *Int. J. Hydrog. Energy*, **33**, 5375 (2008).
39. M. V. Rao, J. Fleig, M. Zinkevich, and F. Aldinger, *Solid State Ionics*, **181**, 1170 (2010).
40. M. Vogler, A. Bieberle-Hutter, L. Gauckler, J. Warnatz, and W. G. Bessler, *J. Electrochem. Soc.*, **156**, B663 (2009).
41. M. J. Escudero, A. Aguadero, J. A. Alonso, and L. Daza, *J. Electroanal. Chem.*, **611**, 107 (2007).
42. B. Ge, J. T. Ma, D. S. Ai, C. S. Deng, X. P. Lin, and J. M. Xu, *Electrochim. Acta*, **151**, 437 (2015).
43. C. Benndorf, C. Nobl, M. Rusenberg, and F. Thieme, *Applications of Surface Science*, **11–2**, 803 (1982).
44. C. Benndorf, C. Nobl, and F. Thieme, *Surf. Sci.*, **121**, 249 (1982).
45. A. Gorski, V. Yurkiv, D. Starukhin, and H. R. Volpp, *J. Power Sources*, **196**, 7188 (2011).
46. C. Jin, C. H. Yang, F. Zhao, D. Cui, and F. L. Chen, *Int. J. Hydrog. Energy*, **36**, 3340 (2011).